Cell Reports

Inactivation of the Medial Entorhinal Cortex Selectively Disrupts Learning of Interval Timing

Graphical Abstract

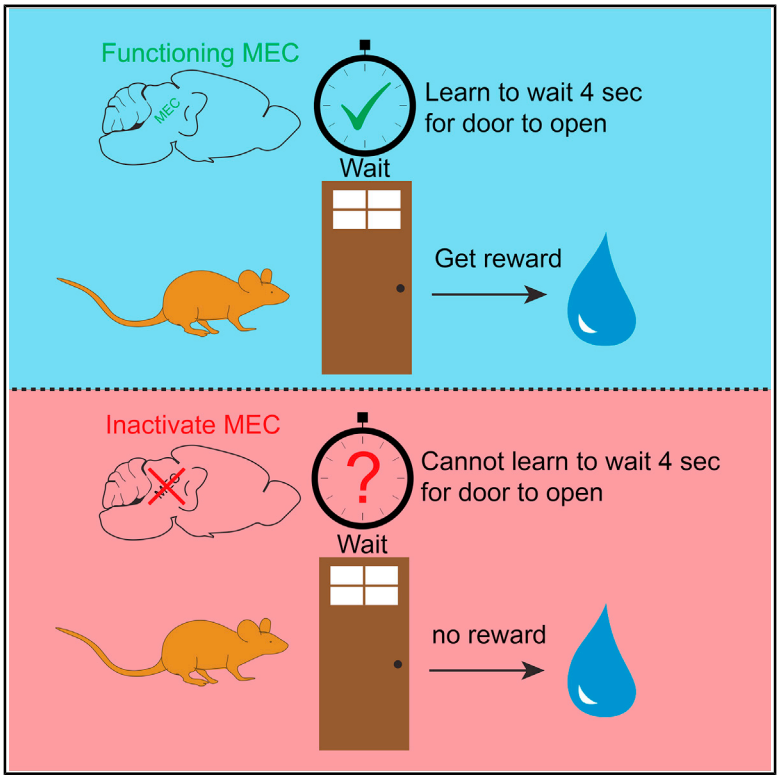

Authors

James G. Heys, Zihan Wu, Anna Letizia Allegra Mascaro, Daniel A. Dombeck

Correspondence

d-dombeck@northwestern.edu

In Brief

Heys et al. investigate the role of the medial entorhinal cortex (MEC) in an explicit interval timing task. Inactivation of the MEC reveals its role in learning interval timing behavior. The results suggest that a MEC subcircuit plays a specific role in learning of interval timing through sequential neural activation during immobility.

Highlights

- Mice learn interval timing task and report duration through immobile waiting
- Optogenetic inactivation of MEC disrupts learning of interval timing behavior
- Learning deficit revealed by MEC inactivation specifically during timing behavior
- MEC inactivation does not significantly impair timing behavior after learning

Heys et al., 2020, Cell Reports *32*, 108163
September 22, 2020
https://doi.org/10.1016/j.celrep.2020.108163

Cell Reports

CellPress
OPEN ACCESS

Report

Inactivation of the Medial Entorhinal Cortex Selectively Disrupts Learning of Interval Timing

James G. Heys,[1,2] Zihan Wu,[1] Anna Letizia Allegra Mascaro,[1,3,4] and Daniel A. Dombeck[1,5,*]
[1]Department of Neurobiology, Northwestern University, Evanston, IL, USA
[2]Present address: Department of Neurobiology and Anatomy, University of Utah, Salt Lake City, UT, USA
[3]Present address: European Laboratory for Non-linear Spectroscopy, Florence, Italy
[4]Present address: Neuroscience Institute, National Research Council, Pisa, Italy
[5]Lead Contact
*Correspondence: d-dombeck@northwestern.edu
https://doi.org/10.1016/j.celrep.2020.108163

SUMMARY

The entorhinal-hippocampal circuit can encode features of elapsed time, but nearly all previous research focused on neural encoding of "implicit time." Recent research has revealed encoding of "explicit time" in the medial entorhinal cortex (MEC) as mice are actively engaged in an interval timing task. However, it is unclear whether the MEC is required for temporal perception and/or learning during such explicit timing tasks. We therefore optogenetically inactivated the MEC as mice learned an interval timing "door stop" task that engaged mice in immobile interval timing behavior and locomotion-dependent navigation behavior. We find that the MEC is critically involved in learning of interval timing but not necessary for estimating temporal duration after learning. Together with our previous research, these results suggest that activity of a subcircuit in the MEC that encodes elapsed time during immobility is necessary for learning interval timing behaviors.

INTRODUCTION

Lesion experiments demonstrate that the hippocampus and entorhinal cortex are necessary for formation of episodic memories (i.e., memories of specific personal experiences that occur in a spatial and temporal context) (Scoville and Milner, 1957; Gaffan, 1974; Mishkin, 1978; Tulving, 1984; Morris et al., 1982; Fortin et al., 2004). In concert with these lesion studies, neurophysiological recordings from awake behaving animals demonstrate that neurons in the hippocampus and entorhinal cortex encode information about animal position in an environment (O'Keefe and Dostrovsky, 1971; Hafting et al., 2005). There is mounting evidence that these neural representations of space serve to encode spatial aspects of episodic memories (Muller and Kubie 1987; Louie and Wilson, 2001; Jadhav et al., 2012; Buzsáki and Moser, 2013). More recently, it has been shown that neurons across the hippocampus and entorhinal cortex encode elapsed time as animals are engaged in memory-guided behaviors (Meck et al., 1984; Fortin et al., 2004; Pastalkova et al., 2008; MacDonald et al., 2011; Naya and Suzuki, 2011; Jacobs et al., 2013; Mankin et al., 2012, 2015; Kraus et al., 2013, 2015; Kitamura et al., 2014; Cai et al., 2016; Deuker et al., 2016; DuBrow and Davachi, 2016; Tsao et al., 2018; Heys and Dombeck, 2018; Sabariego et al., 2019). Although this work has clearly revealed that the entorhinal-hippocampal circuit is capable of encoding features of elapsed time, nearly all previous work has focused on questions regarding how the neural dynamics might encode "implicit time" during behaviors where animals are not actively engaged in memory-guided timing behaviors, such as interval timing. In this view, the function of temporal encoding in the entorhinal-hippocampal circuit is to bridge information across time or provide a neural mechanism for sequential ordering of events through time. In contrast, experiments in our previous work revealed that populations of time-encoding neurons in the medial entorhinal cortex track elapsed time as mice are actively engaged in an interval timing task (Heys and Dombeck, 2018). In this view, the medial entorhinal cortex (MEC) may also serve to encode explicit time as mice are actively engaged in interval timing. Following this work, we sought to determine whether the MEC is necessary for learning interval timing. Previously established models of the MEC, which focused almost exclusively on spatial encoding, would predict that disruption of the MEC in a timing task would have no effect on interval timing behavior. Furthermore, models of the entorhinal-hippocampal circuit that incorporate functions of temporal processing but focus exclusively on a role in implicit timing also predict that these structures do not play a role in interval timing. However, here we demonstrate that inactivation of the MEC produces a selective deficit in the learning of interval timing, establishing that the MEC is involved in the learning of spatial and temporal information and that this role in time encoding is not limited to implicit time.

RESULTS

To inactivate large volumes of the MEC, we leveraged the inhibitory opsin JAWs (Chuong et al., 2014) and Lambda-B tapered optical fibers, which emit light from the entire tapered region of the fiber (Figures 1A and 1B; Pisanello et al., 2018). To deliver light

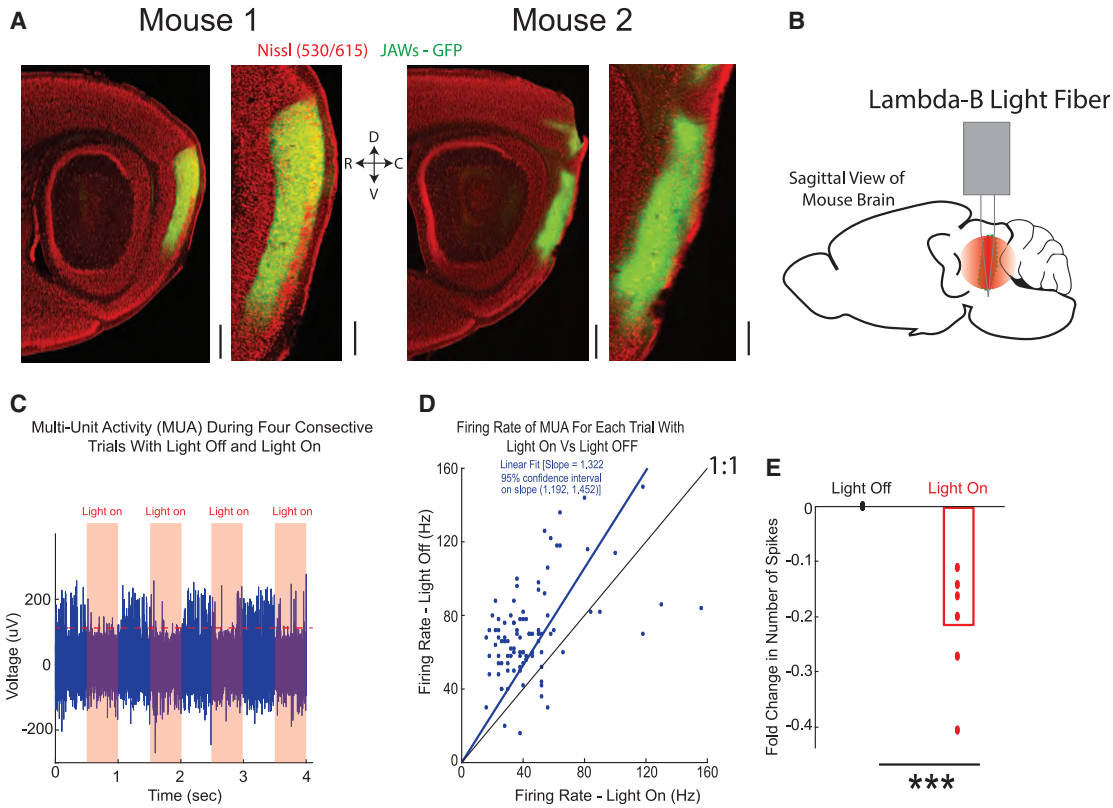

Figure 1. Optogenetically Mediated Inactivation of the MEC

(A) Epifluorescence images of sagittal MEC sections showing expression of JAWs (green) and post hoc staining with fluorescent cell body Nissl stain (red). Scale bars indicate 1 mm for low-magnification (left) and 200 μm for high-magnification (right) images.

(B) Schematic displaying the location of the chronic fiber implant and light delivery methods via Lambda-B fiber. Lambda-B fibers emit light across the entire tapered region of the fiber, which covers the dorsal-ventral extent of the MEC.

(C) Effect of light delivery on multi-unit activity on four consecutive trials from a head-fixed behaving mouse.

(D) Plot of spike frequency for consecutive light-on versus light-off trials across 1 full recording session. 95% confidence interval on slope (1.192, 1.452).

(E) Average change in the number of spikes during light-on versus light-off trials across 6 recording sessions in 4 mice. ***$p < 0.01$, Student's paired t test.

across the dorsal-ventral extent of the MEC, the tapered regions of the Lambda-B fibers were designed to match the dorsal-ventral extent of the mouse MEC. The efficacy of optogenetically mediated inhibition was then tested through multi-unit electrophysiological recordings in the MEC during Lambda-B-mediated light delivery (STAR Methods). We found that this optogenetic approach produced a significant reduction in the multi-unit firing rate across individual trials of light delivery (Figures 1C and 1D) and a 21. 5 ± 0.4% ($p < 0.01$; Student's paired t test, mean ± SEM, n = 6 sessions) decrease in the multi-unit firing rate averaged across all electrode penetrations across 4 mice (Figure 1E).

With the ability to optogenetically inactivate large volumes of the MEC, we sought to determine whether MEC activity was necessary for learning of our previously developed virtual reality-based "door stop" task (Figure 2A) (Heys and Dombeck, 2018). In the door stop task, mice learn to navigate in a virtual environment to a door located halfway down a linear 2-m track through instrumental conditioning (Figure 2A). As mice stop at the door, an auditory click indicates the start of a timer, and the mice are required to remain immobile and wait for a given time interval before the door opens. When the door opens, the mice can run to the end of the 2-m track to obtain a water reward. Therefore, the door stop task engages mice in explicit interval timing behavior as mice learn to wait for a given temporal duration at the door. Before behavioral training, JAWs (AAV-hSyn-JAWs-EGFP, n = 10 mice) was expressed across the dorsal-ventral and medial-lateral extent of both hemispheres of the MEC through virally mediated local injections (Figure 1A). Following these injection surgeries, Lambda-B fibers were chronically implanted bilaterally into the MEC (STAR Methods). In a separate control group, mice were injected in the same way with a control virus (AAV-hSyn-EGFP, n = 8 mice) and implanted bilaterally with Lambda-B fibers. In our task design, the experimenter was blinded to the identity of the control and JAWs groups.

Mouse training began using a 2-s, visible-door version of the door stop task (50 min/training session; STAR Methods; Figure 2A) with no light delivery through the Lambda-B fiber. During this training phase, mice learned how to control their movement through the virtual environment and how to stop at the timing door. Upon reaching criteria on this 2-s version of the door stop task (1 reward/min; ~8 pretraining sessions), the

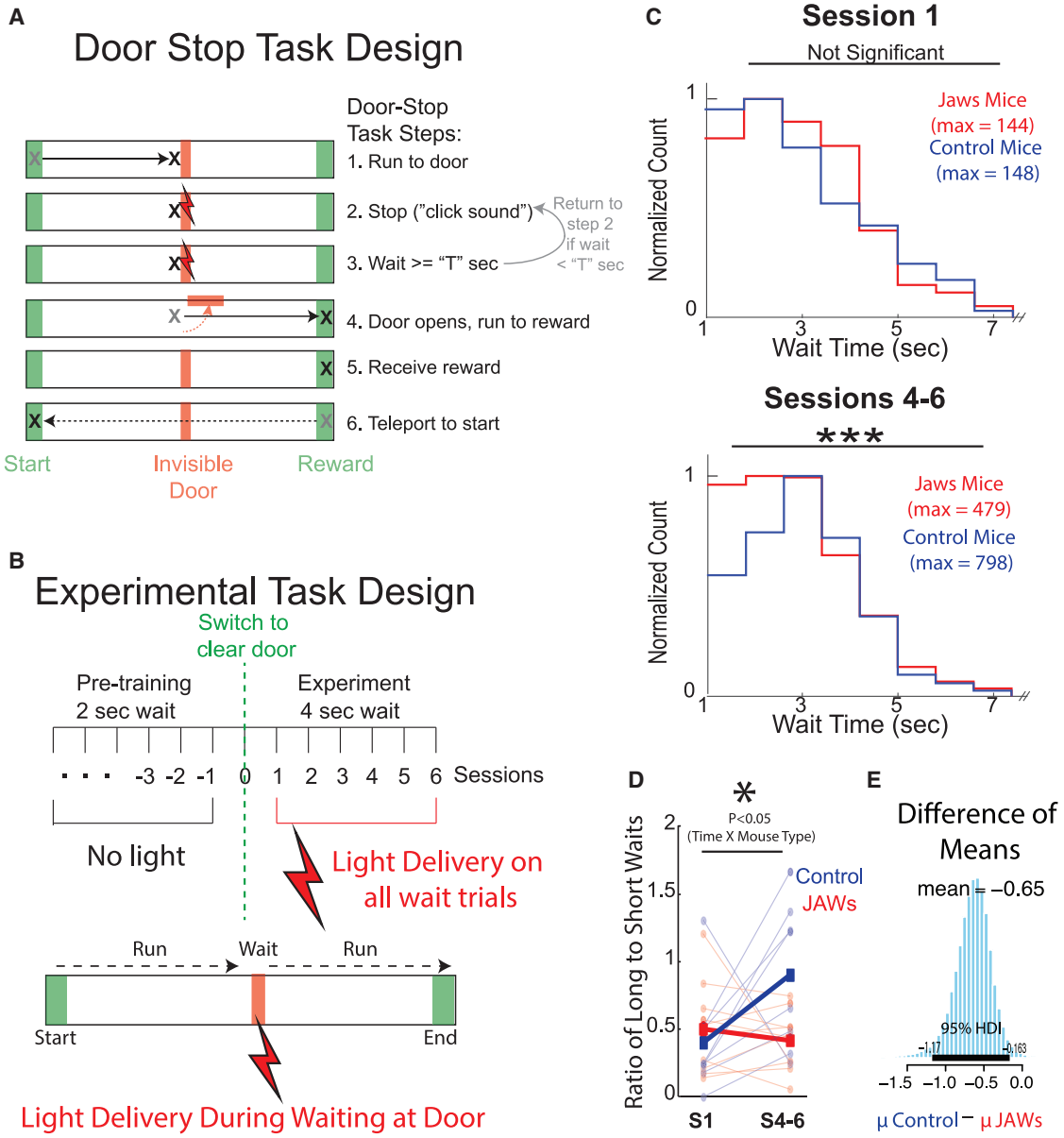

Figure 2. Optogenetically Mediated Inhibition of the MEC during Learning of the Explicit Interval Timing Door Stop Task with Light Delivery during the Timing Period

(A) The virtual door stop task. X indicates the position of the mouse, and a red lightning bolt indicates when light delivery occurred during the task.

(B) Learning paradigm. Mice were first pre-trained on a 2-s visible-door version of the door stop task. Upon reaching criteria (1 rew/min), the experimental phase of the task began (4-s wait at the invisible door), and light was delivered during all periods when the mouse was stopped, waiting at the door.

(C) Wait time distribution across all JAWs mice (n=10) and control mice (n=8) during learning in the 4-s invisible-door door stop task in session 1 (top), control: 2.80 +/- 0.07 s, n = 636; JAWs: 2.98 +/- 0.07 s, n = 634; p = 0.25, Z value = 1.14, rank sum test, median +/- SEM, and sessions 4–6 (bottom), control: 3.04 +/- 0.02 s, n = 2849; JAWs: 2.76 +/- 0.03 s, n = 2042; p = 2.0E-9, Z value = -6.0, rank sum test, median +/- SEM.

(D) Ratio of long to short wait trials for each mouse across session 1 and sessions 4–6. Thick boxes indicate means for each group. $F_{stat} = 5.23$, $p < 0.05$ for group type x time, df = 16; repeated-measures ANOVA.

(E) Bayesian estimates of the fractional change in long to short waits across session 1 to sessions 4–6. HDI (-1.17, -0.16).

experimental phase of the task began. In this phase of the experiment, the task parameters were altered so that the mice were required to wait at an invisible door for 4 s for the invisible door to open (50 min/session). Because the mice could not see the invisible door opening at the end of the 4-s interval, this phase of the task required an internal temporal representation for efficient completion. To determine whether MEC activity is required for learning this timing task, we delivered light though the Lambda-B fiber during all waiting periods at the door. The waiting behavior in this task consisted of two largely non-overlapping

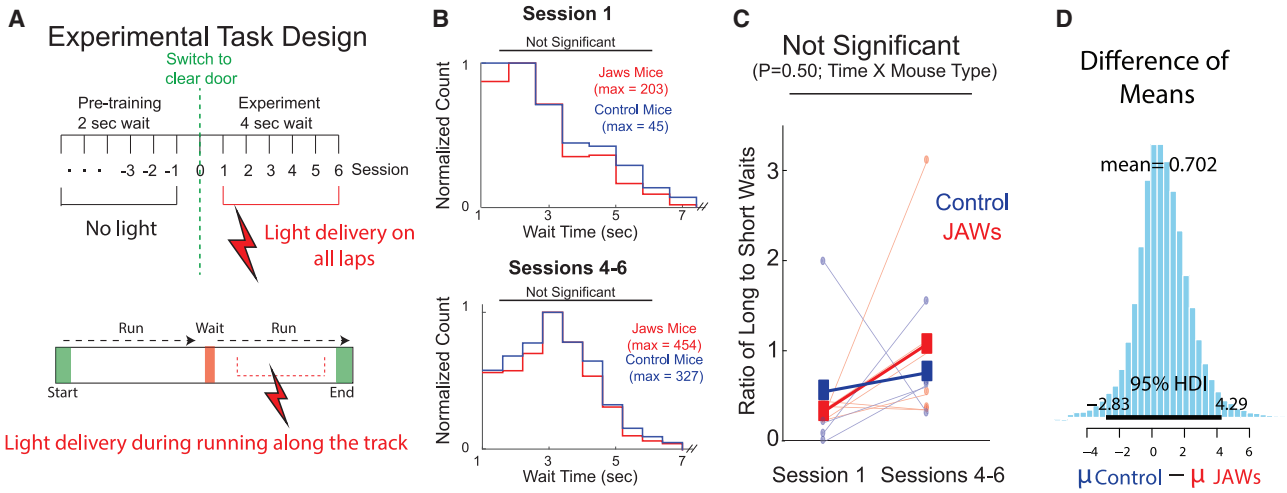

Figure 3. Optogenetically Mediated Inhibition of the MEC during Learning of the Explicit Interval Timing Door Stop Task with Light Delivery during Running along the Track

(A) Learning paradigm. Mice were first pre-trained on a 2-s, visible-door version of the door stop task. Upon reaching criteria (1 rew/min), the experimental phase of the task began (4-s wait at the invisible door), and light was delivered during periods when the animal was running between the door and the reward location.

(B) Wait time distribution across all JAWs mice (n = 6) and control mice (n = 4) during learning on the 4-s invisible-door door stop task in session 1 (top), control: 2.68 +/- 0.13 s, n = 191; JAWs: 2.56 +/- 0.05 s, n = 736; p = 0.12, Z value = -1.56, rank sum test, median +/- SEM, and sessions 4–6 (bottom), control: 3.16 +/- 0.03 s, n = 1710; JAWs: 3.12 +/- 0.03 s, n = 2140; p = 0.08, Z value = -1.75, rank sum test, median +/- SEM.

(C) Ratio of long to short wait trials for each mouse across session 1 and sessions 4–6. Thick boxes indicate means for each group. F_{stat}= 0.49, p = 0.5 for group type x time, df = 8; repeated-measures ANOVA.

(D) Bayesian estimates of the fractional change in long to short waits across session 1 to session 4–6. HDI (-2.83, 4.29).

distributions: (1) a timing component with a more than 1-s wait period and (2) a non-timing component that resulted from above-threshold velocity crossing as the mice slowed upon reaching the door location and short-duration jerky movements while waiting at the door (Figures S1A and S1B). Given the separation of these distributions, our analysis focused on the more than 1-s wait periods consistent with timing behavior. This was implemented over 6 separate sessions for each mouse, and the wait times at the door in each trial were quantified and used as a measure of learning. We found that the median wait time of the control and JAWs groups was not significantly different during the first behavioral session (control, 2.80 ± 0.07 s, n = 636 trials; JAWs, 2.98 ± 0.07 s, n = 634 trials; p = 0.25, Z value = 1.14, rank-sum test, median ± SEM) (Figure 2C, top; Figure S1C, left). However, after several sessions of training on the task, the median wait time was significantly longer for the control group compared with the JAWs group (sessions 4–6: control, 3.04 ± 0.02 s, n = 2,849; JAWs, 2.76 ± 0.03 s, n = 2,042; p = 2.0E−9, Z value = −6.0, rank-sum test, median ± SEM) (Figure 2C, bottom; Figure S1C, right). To further quantify this change in timing behavior, we compared the ratio of long to short waits for each mouse on session 1 with sessions 4–6 of training (1 s < short waits < 2.5 s; 3.5 s < long waits < 4.5 s). The results demonstrate a significant effect of group type × time (F_{stat} = 5.23, p < 0.05 for group type × time, df = 16, repeated-measures ANOVA) (Figure 2D), and this result was confirmed using Bayesian estimation to compute the posterior distribution of differences in means of the fractional change in long/short wait ratios across the control and JAWs groups (0 is not contained in the 95% highest-density interval [HDI]; mean difference = −0.65; HDI [−1.17, −0.16]) (Figure 2E).Therefore, our results demonstrate that inactivation of the MEC disrupts learning of an explicit interval timing task.

In a second series of experiments, we sought to determine whether the learning deficit observed in JAWs mice was caused specifically by inactivating the MEC as mice were waiting at the door during immobile timing behavioral epochs. We reasoned that it is possible that inactivation of the MEC during any behavioral epoch during the door stop task might be sufficient to disrupt learning of the interval timing task. We therefore performed a separate set of experiments in which the MEC was inactivated during the spatial phase of the task when mice were running down the track. Again, the experimenter was blinded to mouse identity (n = 6 JAWs mice, n = 4 EGFP control mice). Training began using the 2-s wait solid-door door stop task (50 min/training session) without light delivery (Figure 3A). When mice reached criteria, they were moved to the experimental phase of the task (4-s wait with an invisible door), and light was delivered during periods of locomotion between the door and the reward location (50 min/session). To closely match the duration of light delivery during locomotion to the duration used in the previous experiment, in which light was delivered while mice were waiting at the door, we first calculated the mean light duration during door waiting (mean = 3.33 s). Then the duration of light delivery during locomotion in each trial was chosen randomly from an exponential distribution using this mean value. This light delivery was implemented over 6 separate sessions for each mouse, and again the door wait times in each trial were quantified and used as a measure of learning. For this set of experiments, in which light was delivered during locomotion, we

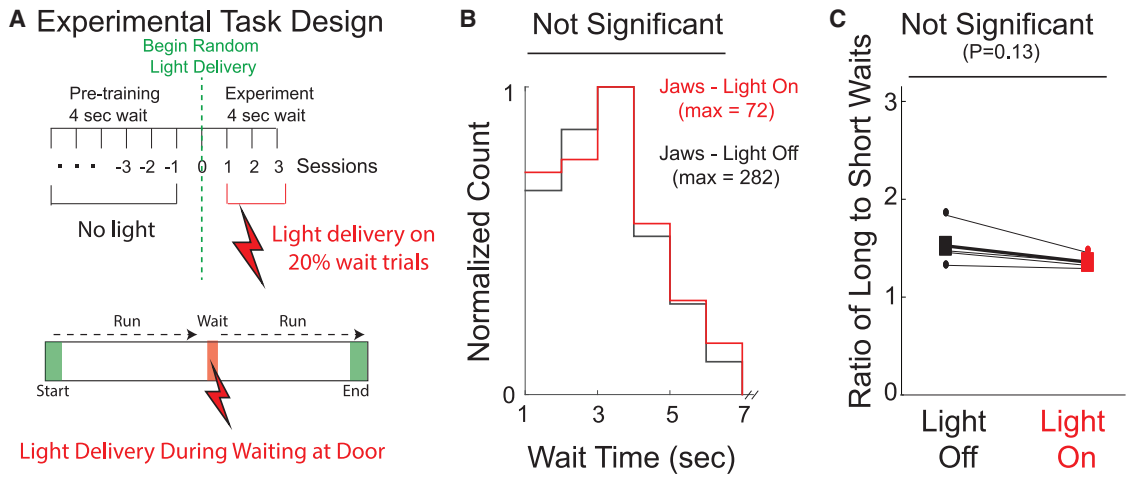

Figure 4. Optogenetically Mediated Inhibition of the MEC after Learning the Explicit Interval Timing Door Stop Task with Light Delivery while Waiting at the Door in a Random Subset of Trials

(A) Learning paradigm. Mice were first pre-trained for 7 training sessions on a 4-s invisible-door version of the door stop task. In experimental sessions 1–3, light was delivered during a random subset (20%) of wait trials while mice waited at the door.

(B) Wait time distribution across all JAWs mice during light-on trials (red) and light-off trials (black), averaged across 4 mice for all behavioral sessions. Light On: 3.28 +/- 0.10 s, n = 264; Light Off: 3.28 +/- 0.05 s, n = 1010; p = 0.87, Z value = 0.16, rank sum test, median +/- SEM.

(C) Ratio of long to short wait trials for each mouse during light-on (red) and light-off trials (black). Thick boxes indicate means for each group. p = 0.13, paired signed-rank test.

found that the median wait time of the control and JAWs groups was not significantly different during the first behavioral session (control: 2.68 ± 0.13 s, n = 191 trials; JAWs: 2.56 ± 0.05 s, n = 736 trials; p = 0.12, Z value = −1.56, rank-sum test (median ± SEM) (Figure 3B, top) or after 4–6 sessions of training on the door stop task (control: 3.16 ± 0.03 s, n = 1,710 trials; JAWs: 3.12 ± 0.03 s, n = 2,140 trials; p = 0.08, Z value = −1.75, rank-sum test (median ± SEM) (Figure 3B, bottom). To test the precision of timing, we compared the dispersion of the wait time distributions. The results show that there is no significant difference in the variance between control and JAWs mice for sessions 4–6 (F_{stat} = 1.07, df_{num} = 1,665, df_{denom} = 2,121, p = 0.135). Using a within-mouse comparison, we did not observe a significant effect of group type × time when comparing the ratio of long to short wait times for the JAWs and control groups across time (F_{stat} = 0.49, p = 0.50 for group type × time, df = 8, repeated-measures ANOVA) (Figure 3C). Furthermore, we found that there was no significant effect when using Bayesian estimation to compute the posterior distribution of differences in means of the fractional change in long/short wait ratios across control and JAWs groups (0 is contained in the HDI; mean difference = 0.702; HDI [−2.83, 4.29]) (Figure 3D). In contrast, there was a significant effect of group type × time when comparing the ratio of long to short wait times across time for JAWs (light at the door) versus JAWs (light along the track) groups (F_{stat} = 5.30, p < 0.05 for group type × time, df = 14, repeated-measures ANOVA). Thus, the disruption of interval time learning observed when inhibiting the MEC during the interval timing epochs of the door stop task is not observed when inhibiting the MEC during the spatial navigation phase of the same task.

The results above demonstrate that the MEC is critically involved in the learning phase of the door stop task. In addition to a role in learning, it is possible that the MEC may also play a role in "on-line" estimation (perception) of duration after learning has occurred. To address this question, JAWs-expressing mice (n = 5 mice) were trained on the 4-s version of the invisible-door door stop task without light delivery for 7 sessions (50 min/training session), resulting in learning the task (~0.5 rewards/min). Following this training period, optogenetic inactivation experiments began by delivering light in a random 20% of trials throughout the behavioral session for a total of 3 sessions (50 min/session) (Figure 4A). To assess the effect of MEC inactivation, the wait time distribution at the door was measured during light-on and light-off trials. We found that there was no detectable effect of MEC inactivation on the wait time distribution after learning had already taken place (light on: 3.28 ± 0.10 s, n = 264 trials; light off: 3.28 ± 0.05 s, n = 1,010 trials; p = 0.87, Z value = 0.16, rank-sum test, median ± SEM) (Figure 4B). Accordingly, comparison of the ratio of long to short waits showed no significant effect on wait time between light-on and light-off trials (light on: 0.68 ± 0.02; light off: 0.77 ± 0.05, n = 4 mice; p = 0.13, paired signed-rank test (mean ± SEM) (Figure 4C). Therefore, after learning an interval timing task, inactivation of the MEC does not appear to alter the on-line estimation of duration.

DISCUSSION

Here we establish a role of the MEC in learning explicit interval timing behavior. Furthermore, we observe selective disruption of learning of interval timing behavior by inhibiting the MEC specifically during behavioral epochs when mice are engaged in immobile timing behavior but not when mice are engaged in the locomotion-dependent navigation phase of the door stop

task. This research is a departure from previous studies of the entorhinal cortex and hippocampus that have focused on temporal encoding in the context of implicit timing. This previous research focused on how populations of neurons across the hippocampus and entorhinal cortex could encode information about stimuli across temporal delays during working memory tasks or how these structures could serve to encode a sequential order of events (Pastalkova et al., 2008; MacDonald et al., 2011; Naya and Suzuki, 2011; Suh et al., 2011; Mankin et al., 2012, 2015; Jacobs et al., 2013; Kraus et al., 2013, 2015; Kitamura et al., 2014; Cai et al., 2016; Deuker et al., 2016; DuBrow and Davachi, 2016; Tsao et al., 2018; Sabariego et al., 2019). In concert with a role in implicit temporal coding, our experiments here demonstrate that the MEC also plays a role in learning explicit interval timing behaviors.

Previous lesion studies aimed at uncovering the neural substrates of timing have largely focused on corticostriatal and cerebellar circuits. Several comprehensive reviews have summarized this research (Ivry and Schlerf, 2008; Coull et al., 2011; Merchant et al., 2013; Allman et al., 2014). Regarding the MEC itself, the vast majority of studies have described a primary role of the MEC in coding spatial information. Importantly, these studies designed instrumental behavioral tasks in which spatial memory is imperative, and in many studies, reward is contingent only on spatial location. However, in studies that developed behavioral paradigms that explicitly required animals to encode non-spatial behavioral variables, the MEC was found to form neural representations of these non-spatial variables, including time (Aronov et al., 2017; Heys and Dombeck, 2018). Furthermore, previous lesion work using trace conditioning tasks provided evidence that the MEC could be involved more broadly in temporal association (Ryou et al., 2001; Esclassan et al., 2009; Morrissey et al., 2012). Previous lesion studies have also shown that entorhinal cortical lesions can produce hyperactivity in rodents (Ross et al., 1973; Schenk et al., 1983). Based on these observations, an alternative hypothesis to account for the results in our study is that entorhinal inactivation increases hyperactive and impulsive behavior, resulting in more short waits trials, while leaving interval timing intact. To address this alternative explanation for the behavioral deficits seen in our study, mouse velocity was analyzed during light delivery while waiting at the door (Figures S2A–S2C) and during light delivery while running along the track (Figures S2D–S2F). If MEC inactivation increased mouse impulsivity, one of the likely behavioral correlates would be an increased number of sub-threshold movements in JAWs mice. In addition, impulsivity would be expected to change the mean running velocity. However, in both cases (sub-threshold movement and running velocity), we find that there are no significant differences between the control and JAWs groups (Figures S2C and S2F). Finally, previous literature regarding hyperactivity caused by entorhinal lesion suggests that this behavioral phenotype should persist after learning. However, we observed no difference in mouse timing behavior during MEC inactivation after learning occurred (Figure 4).

A variety of psychological and neurobiological models have been put forth to account for interval timing on the scale of many seconds. A large class of models, referred to as pacemaker-accumulator models, use some form of an accumulator/integrator mechanism that counts "pulses" produced by a pacemaker and compares the accumulated total with a reference/threshold value to estimate duration (Creelman, 1962; Treisman, 1963; Killeen and Fetterman, 1988; Gibbon, 1977; Gibbon and Church, 1984; Gibbon et al., 1984). These models were originally described in abstract terms and have now evolved to include more physiological details (Matell and Meck, 2004; Simen et al., 2011, 2016) and produce variation in temporal estimates through two essential mechanisms: changing the value of the reference/threshold or changing the rate of pulses (Balci and Simen, 2016). Importantly, these different mechanisms lead to different predictions of timing behavior that could be tested empirically. For example, the behavioral theory of timing, the scalar expectancy theory, and the opponent Poisson diffusion model of interval timing predict that timing behavior in a peak interval task (similar to our door stop task) should produce gamma, normal, and inverse Gaussian timing distributions, respectively. The timing behavior observed among control mice after several training sessions in our door stop task can be approximated by a Gaussian (Figure S1) but also well fit with inverse Gaussian and gamma distributions; future research with greater sampling (e.g., a greater number of trials per session) may be better able to distinguish between these distributions. Another prediction from the opponent Poisson diffusion model is that learning new temporal estimates should occur relatively rapidly with discrete jumps (Simen et al., 2011). This model prediction is consistent with previously published behavioral results in rodents (Meck et al., 1984; Davis et al., 1989; Bevins and Ayres, 1995). In light of this modeling result, one prediction is that inactivating timing circuits earlier in training may preferentially disrupt learning of timing behavior. Although the experiments in our study were not designed to address this question, future work could more precisely explore the dynamics of MEC inactivation in learning timing behavior. Another class of models proposes that interval timing could arise through sequential activity produced by training of randomly recurrent neural networks (Buonomano and Merzenich 1995; Maass et al., 2002; Laje and Buonomano, 2013; Hardy et al., 2018). These models can produce a variety of timing distributions based on the specifics of the training, making it difficult to empirically rule in or out these models by measuring timing distributions.

Here, when the MEC was inactivated during our timing task but after learning had taken place, we found no detectable effect on the animal's timing behavior, suggesting that the MEC does not play a critical role in on-line estimation of duration during interval timing. However, this result leaves open many questions and possibilities regarding the role of the MEC in learning and perception of time intervals. For example, it is possible that the temporal representations found in the MEC during learning form the basis of temporal perception required for interval time learning (Heys and Dombeck, 2018). However, after learning, other brain systems (the striatum, other cortical regions, etc.) could form the temporal representations required for time perception and task execution, possibly through training by the MEC. In this scenario, the MEC representations observed after learning (Heys and Dombeck, 2018) could still form part of the perception of elapsed time but are not required for it because redundant representations exist across other brain regions.

Such a scenario could occur through mechanisms similar to those thought to underlie hippocampal-cortical memory transfer (Frankland and Bontempi, 2005). Alternatively, temporal representations forming the basis of the perception of time might be generated outside of the MEC. Instead, the role of the MEC may be to aid with formation of memories that incorporate copies of these temporal representations. In this scenario, MEC inactivation would inhibit learning, but the MEC representations observed after learning (as seen in Heys and Dombeck, 2018) would not be required for perception of elapsed time. Interestingly, similar open questions and possibilities exist regarding the role of the hippocampal-entorhinal circuitry in spatial learning and online spatial perception. For example, selective lesions to the MEC or hippocampus often lead to deficits in spatial learning (Morris et al., 1982; Steffenach et al., 2005), but in retention experiments where lesions were applied to the hippocampus after spatial learning had already occurred, spatial memory was not different between the lesion and sham groups (Morris et al., 1982). However, retention experiments where lesions were applied to the MEC after spatial learning had already occurred showed deficits in spatial memory in the lesion compared with the sham groups on a single probe trial, but the differences were abolished after many trials (Steffenach et al., 2005).

The inactivation experiments presented here, together with our previous findings (Heys and Dombeck, 2018), have direct implications for sub-circuits in the MEC that could differentially mediate learning of time and space during immobility and locomotion, respectively. In our previous experiments, time-encoding neurons in the MEC were selectively active during periods of immobile timing at the door and far less active during periods of locomotion as mice were navigating along the track. In contrast, space-encoding neurons tended to be active during locomotion bouts while mice were running along the track and far less active during immobile timing periods at the door. Temporal versus spatial encoding neurons in the MEC also displayed a predisposition for encoding time or space, respectively, across distinct environments and across completely different behavioral tasks. Furthermore, the temporal representations in the MEC were present from the first moments after animals were placed in novel environments. Based on these findings, our previous work suggests the existence of largely non-overlapping functional sub-circuits in the MEC that encode time during animal immobility or space during animal locomotion. Together, the results presented here, along with our previous research, suggest that it is the activity of this immobile timing circuit in the MEC that is critical for learning interval timing in our behavioral task.

STAR★METHODS

Detailed methods are provided in the online version of this paper and include the following:

- KEY RESOURCES TABLE
- RESOURCE AVAILABILITY
  - Lead Contact
  - Materials Availability
  - Data and Code Availability
- EXPERIMENTAL MODEL AND SUBJECT DETAILS
- METHOD DETAILS
  - Viral Vector and Optical Fiber Implant Surgeries
  - Behavior
  - Pre-training Phase - linear track (no Door Stop) followed by a 2 s visible Door Stop task:
  - Experimental Phase – 4 s Invisible Door Stop Task
  - Optical inhibition of MEC neurons
  - Histology
- QUANTIFICATION AND STATISTICAL ANALYSIS
  - Statistical Tests
  - Data Analysis

SUPPLEMENTAL INFORMATION

Supplemental Information can be found online at https://doi.org/10.1016/j.celrep.2020.108163.

ACKNOWLEDGMENTS

We thank C. Woolley for use of the freezing microtome and G. Kozorovitskiy for the use of the slide scanning microscope. This work was supported by The McKnight Foundation (to D.A.D.), a post-doctoral fellowship from The Simons Collaboration on the Global Brain (to J.G.H.), The Chicago Biomedical Consortium with support from the Searle Foundation at The Chicago Community Trust (to D.A.D.), and the NIH (2R01MH101297 to D.A.D.).

AUTHOR CONTRIBUTIONS

J.G.H. designed and performed experiments, conducted analyses, and wrote the manuscript. Z.W. and A.L.A.M. performed experiments. D.A.D. designed experiments, conducted analyses, and wrote the manuscript.

DECLARATION OF INTERESTS

The authors declare no competing interests.

Received: September 19, 2019
Revised: March 6, 2020
Accepted: August 26, 2020
Published: September 22, 2020

REFERENCES

Allman, M.J., Teki, S., Griffiths, T.D., and Meck, W.H. (2014). Properties of the internal clock: first- and second-order principles of subjective time. Annu. Rev. Psychol. *65*, 743–771.

Aronov, D., Nevers, R., and Tank, D.W. (2017). Mapping of a non-spatial dimension by the hippocampal-entorhinal circuit. Nature *543*, 719–722.

Balci, F., and Simen, P. (2016). A decision model of timing. Curr. Opin. Behav. Sci. *8*, 94–101.

Bevins, R., and Ayres, J.J.B. (1995). One-trial context fear conditioning as a function of the interstimulus interval. Anim. Learn. Behav. *23*, 400–410.

Buonomano, D.V., and Merzenich, M.M. (1995). Temporal information transformed into a spatial code by a neural network with realistic properties. Science *267*, 1028–1030.

Buzsáki, G., and Moser, E.I. (2013). Memory, navigation and theta rhythm in the hippocampal-entorhinal system. Nat. Neurosci. *16*, 130–138.

Cai, D.J., Aharoni, D., Shuman, T., Shobe, J., Biane, J., Song, W., Wei, B., Veshkini, M., La-Vu, M., Lou, J., et al. (2016). A shared neural ensemble links distinct contextual memories encoded close in time. Nature *534*, 115–118.

Chuong, A.S., Miri, M.L., Busskamp, V., Matthews, G.A., Acker, L.C., Sørensen, A.T., Young, A., Klapoetke, N.C., Henninger, M.A., Kodandaramaiah,

S.B., et al. (2014). Noninvasive optical inhibition with a red-shifted microbial rhodopsin. Nat. Neurosci. *17*, 1123–1129.

Coull, J.T., Cheng, R.K., and Meck, W.H. (2011). Neuroanatomical and neurochemical substrates of timing. Neuropsychopharmacology *36*, 3–25.

Creelman, C.D. (1962). Human discrimination of auditory duration. J. Acoust. Soc. Am. *34*, 582–593.

Davis, M., Schlesinger, L.S., and Sorenson, C.A. (1989). Temporal specificity of fear conditioning: effects of different conditioned stimulus-unconditioned stimulus intervals on the fear-potentiated startle effect. J. Exp. Psychol. Anim. Behav. Process. *15*, 295–310.

Deuker, L., Bellmund, J.L., Navarro Schröder, T., and Doeller, C.F. (2016). An event map of memory space in the hippocampus. eLife *5*, e16534.

Dombeck, D.A., Harvey, C.D., Tian, L., Looger, L.L., and Tank, D.W. (2010). Functional imaging of hippocampal place cells at cellular resolution during virtual navigation. Nat. Neurosci. *13*, 1433–1440.

DuBrow, S., and Davachi, L. (2016). Temporal binding within and across events. Neurobiol. Learn. Mem. *134*, 107–114.

Esclassan, F., Coutureau, E., Di Scala, G., and Marchand, A.R. (2009). A cholinergic-dependent role for the entorhinal cortex in trace fear conditioning. J. Neurosci. *29*, 8087–8093.

Fortin, N.J., Wright, S.P., and Eichenbaum, H. (2004). Recollection-like memory retrieval in rats is dependent on the hippocampus. Nature *431*, 188–191.

Frankland, P.W., and Bontempi, B. (2005). The organization of recent and remote memories. Nat. Rev. Neurosci. *6*, 119–130.

Gaffan, D. (1974). Recognition impaired and association intact in the memory of monkeys after transection of the fornix. J. Comp. Physiol. Psychol. *86*, 1100–1109.

Gibbon, J. (1977). Scalar expectancy theory and Weber's law in animal timing. Psychol. Rev. *84*, 279–325.

Gibbon, J., and Church, R.M. (1984). Sources of variance in an information processing theory of timing. In Animal Cognition, H.L. Roitblat, T.G. Bever, and H.S. Terrace, eds. (Erlbaum), pp. 465–487.

Gibbon, J., Church, R.M., and Meck, W.H. (1984). Scalar timing in memory. Ann. N Y Acad. Sci. *423*, 52–77.

Hafting, T., Fyhn, M., Molden, S., Moser, M.-B., and Moser, E.I. (2005). Microstructure of a spatial map in the entorhinal cortex. Nature *436*, 801–806.

Hardy, N.F., Goudar, V., Romero-Sosa, J.L., and Buonomano, D.V. (2018). A model of temporal scaling correctly predicts that motor timing improves with speed. Nat. Commun. *9*, 4732.

Harvey, C.D., Collman, F., Dombeck, D.A., and Tank, D.W. (2009). Intracellular dynamics of hippocampal place cells during virtual navigation. Nature *461*, 941–946.

Heys, J.G., and Dombeck, D.A. (2018). Evidence for a subcircuit in medial entorhinal cortex representing elapsed time during immobility. Nat. Neurosci. *21*, 1574–1582.

Heys, J.G., Rangarajan, K.V., and Dombeck, D.A. (2014). The functional micro-organization of grid cells revealed by cellular-resolution imaging. Neuron *84*, 1079–1090.

Ivry, R.B., and Schlerf, J.E. (2008). Dedicated and intrinsic models of time perception. Trends Cogn. Sci. *12*, 273–280.

Jacobs, N.S., Allen, T.A., Nguyen, N., and Fortin, N.J. (2013). Critical role of the hippocampus in memory for elapsed time. J. Neurosci. *33*, 13888–13893.

Jadhav, S.P., Kemere, C., German, P.W., and Frank, L.M. (2012). Awake hippocampal sharp-wave ripples support spatial memory. Science *336*, 1454–1458.

Killeen, P.R., and Fetterman, J.G. (1988). A behavioral theory of timing. Psychol. Rev. *95*, 274–295.

Kitamura, T., Pignatelli, M., Suh, J., Kohara, K., Yoshiki, A., Abe, K., and Tonegawa, S. (2014). Island cells control temporal association memory. Science *343*, 896–901.

Kraus, B.J., Robinson, R.J., 2nd, White, J.A., Eichenbaum, H., and Hasselmo, M.E. (2013). Hippocampal "time cells": time versus path integration. Neuron *78*, 1090–1101.

Kraus, B.J., Brandon, M.P., Robinson, R.J., 2nd, Connerney, M.A., Hasselmo, M.E., and Eichenbaum, H. (2015). During Running in Place, Grid Cells Integrate Elapsed Time and Distance Run. Neuron *88*, 578–589.

Kruschke, J. (2015). Doing Bayesian Data Analysis: A Tutorial with R, JAGS, and Stan, Second Edition (San Diego: Academic Press).

Laje, R., and Buonomano, D.V. (2013). Robust timing and motor patterns by taming chaos in recurrent neural networks. Nat. Neurosci. *16*, 925–933.

Louie, K., and Wilson, M.A. (2001). Temporally structured replay of awake hippocampal ensemble activity during rapid eye movement sleep. Neuron *29*, 145–156.

Maass, W., Natschläger, T., and Markram, H. (2002). Real-time computing without stable states: a new framework for neural computation based on perturbations. Neural Comput. *14*, 2531–2560.

MacDonald, C.J., Lepage, K.Q., Eden, U.T., and Eichenbaum, H. (2011). Hippocampal "time cells" bridge the gap in memory for discontiguous events. Neuron *71*, 737–749.

Mankin, E.A., Sparks, F.T., Slayyeh, B., Sutherland, R.J., Leutgeb, S., and Leutgeb, J.K. (2012). Neuronal code for extended time in the hippocampus. Proc. Natl. Acad. Sci. USA *109*, 19462–19467.

Mankin, E.A., Diehl, G.W., Sparks, F.T., Leutgeb, S., and Leutgeb, J.K. (2015). Hippocampal CA2 activity patterns change over time to a larger extent than between spatial contexts. Neuron *85*, 190–201.

Matell, M.S., and Meck, W.H. (2004). Cortico-striatal circuits and interval timing: coincidence detection of oscillatory processes. Brain Res. Cogn. Brain Res. *21*, 139–170.

Meck, W.H., Church, R.M., and Olton, D.S. (1984). Hippocampus, time, and memory. Behav. Neurosci. *98*, 3–22.

Merchant, H., Harrington, D.L., and Meck, W.H. (2013). Neural basis of the perception and estimation of time. Annu. Rev. Neurosci. *36*, 313–336.

Mishkin, M. (1978). Memory in monkeys severely impaired by combined but not by separate removal of amygdala and hippocampus. Nature *273*, 297–298.

Morris, R.G., Garrud, P., Rawlins, J.N., and O'Keefe, J. (1982). Place navigation impaired in rats with hippocampal lesions. Nature *297*, 681–683.

Morrissey, M.D., Maal-Bared, G., Brady, S., and Takehara-Nishiuchi, K. (2012). Functional dissociation within the entorhinal cortex for memory retrieval of an association between temporally discontiguous stimuli. J. Neurosci. *32*, 5356–5361.

Muller, R.U., and Kubie, J.L. (1987). The effects of changes in the environment on the spatial firing of hippocampal complex-spike cells. J. Neurosci. *7*, 1951–1968.

Naya, Y., and Suzuki, W.A. (2011). Integrating what and when across the primate medial temporal lobe. Science *333*, 773–776.

O'Keefe, J., and Dostrovsky, J. (1971). The hippocampus as a spatial map. Preliminary evidence from unit activity in the freely-moving rat. Brain Res. *34*, 171–175.

Pastalkova, E., Itskov, V., Amarasingham, A., and Buzsáki, G. (2008). Internally generated cell assembly sequences in the rat hippocampus. Science *321*, 1322–1327.

Pisanello, M., Pisano, F., Sileo, L., Maglie, E., Bellistri, E., Spagnolo, B., Mandelbaum, G., Sabatini, B.L., De Vittorio, M., and Pisanello, F. (2018). Tailoring light delivery for optogenetics by modal demultiplexing in tapered optical fibers. Sci. Rep. *8*, 4467.

Ross, J.F., Walsh, L.L., and Grossman, S.P. (1973). Some behavioral effects of entorhinal cortex lesions in the albino rat. J Comp Physiol Psychol *85*, 70–81.

Ryou, J.W., Cho, S.Y., and Kim, H.T. (2001). Lesions of the entorhinal cortex impair acquisition of hippocampal-dependent trace conditioning. Neurobiol. Learn. Mem. *75*, 121–127.

Sabariego, M., Schönwald, A., Boublil, B.L., Zimmerman, D.T., Ahmadi, S., Gonzalez, N., Leibold, C., Clark, R.E., Leutgeb, J.K., and Leutgeb, S. (2019).

Time Cells in the Hippocampus Are Neither Dependent on Medial Entorhinal Cortex Inputs nor Necessary for Spatial Working Memory. Neuron *102*, 1235–1248.e5.

Schenk, F., Inglin, F., and Gyger, M. (1983). Activity and exploratory behavior after lesions of the medial entorhinal cortex in the woodmouse (Apodemus sylvaticus). Behav Neural Biol *37*, 89–107.

Scoville, W.B., and Milner, B. (1957). Loss of recent memory after bilateral hippocampal lesions. J. Neurol. Neurosurg. Psychiatry *20*, 11–21.

Simen, P., Balci, F., de Souza, L., Cohen, J.D., and Holmes, P. (2011). A model of interval timing by neural integration. J. Neurosci. *31*, 9238–9253.

Simen, P., Vlasov, K., and Papadakis, S. (2016). Scale (in)variance in a unified diffusion model of decision making and timing. Psychol. Rev. *123*, 151–181.

Steffenach, H.A., Witter, M., Moser, M.B., and Moser, E.I. (2005). Spatial memory in the rat requires the dorsolateral band of the entorhinal cortex. Neuron *45*, 301–313.

Suh, J., Rivest, A.J., Nakashiba, T., Tominaga, T., and Tonegawa, S. (2011). Entorhinal cortex layer III input to the hippocampus is crucial for temporal association memory. Science *334*, 1415–1420.

Treisman, M. (1963). Temporal discrimination and the indifference interval. Implications for a model of the "internal clock". Psychol. Monogr. *77*, 1–31.

Tsao, A., Sugar, J., Lu, L., Wang, C., Knierim, J.J., Moser, M.B., and Moser, E.I. (2018). Integrating time from experience in the lateral entorhinal cortex. Nature *561*, 57–62.

Tulving, E. (1984). Precis of elements of episodic memory. Behav. Brain Sci. *7*, 223–268.

STAR★METHODS

KEY RESOURCES TABLE

REAGENT or RESOURCE	SOURCE	IDENTIFIER
Bacterial and Virus Strains		
AAV8.hSyn.Jaws-KGC.GFP-ER2.WPRE.hGH	Addgene	65014-AAV8
pAAV8-hSyn-EGFP	Addgene	50465-AAV8
Chemicals, Peptides, and Recombinant Proteins		
NeuroTrace 530/615 Red Fluorescent Nissl Stain	Invitrogen	N21482
NeuroTrace 435/455 Blue Fluorescent Nissl Stain	Invitrogen	N21479
Experimental Models: Organisms/Strains		
Mouse: C57-BL6	Charles River	N/A
Software and Algorithms		
MATALB	Mathworks	https://www.mathworks.com/products/MATLAB.html
P-Clamp	Axon Instruments	https://www.moleculardevices.com/

RESOURCE AVAILABILITY

Lead Contact

Further information and requests for resources and reagents should be directed to and will be fulfilled by the Lead Contact, Daniel A. Dombeck (d-dombeck@northwestern.edu)

Materials Availability

This study did not generate new unique reagents.

Data and Code Availability

All datasets and custom analysis scripts generated and used in the current study are available from the Lead Contact

EXPERIMENTAL MODEL AND SUBJECT DETAILS

All mice used in this study were P56-P90 male C57-BL6 (Charles River). Mice were house in reverse light cycle: 12hr dark-12 hour light. All experiments were approved and conducted in accordance with the Northwestern University Animal Care and Use Committee.

METHOD DETAILS

Viral Vector and Optical Fiber Implant Surgeries

To achieve widespread expression of JAWs in MEC neurons, C57-BL6 mice (n = 38 male; postnatal 3–5 months) were injected bilaterally with AAV8.hSyn.Jaws-KGC.GFP-ER2.WPRE.hGH (Addgene: 9.75 × 10^{12} GC ml^{-1}; diluted 2:1 in PBS) or pAAV8-hSyn-EGFP (Addgene: 3.0 × 10^{13} GC ml^{-1}; diluted 2:1 in PBS). In each hemisphere, ~40nl of virus was injected using a beveled pipette positioned at each of the following 7 sites: 2.8 mm lateral from bregma and 150 μm rostral from the transverse sinus, injections were made at three depths along the dorsal-ventral axis (1.2, 1.7 and 2.2 mm from the dorsal surface of the brain); at 3.2 mm lateral from bregma and 350 μm rostral from the transverse sinus, injections were made at three depths along the dorsal-ventral axis (1.2, 1.7 and 2.2 mm from the dorsal surface of the brain); at 3.5mm lateral from bregma and 150 μm rostral from the transverse sinus, injections were made at one depths along the dorsal-ventral axis (1.8 mm from the dorsal surface of the brain). The mice then began water scheduling (receiving ~1mL of water/day) as described previously (Harvey et al., 2009; Dombeck et al., 2010; Heys et al., 2014). 2-4 weeks following the viral injection surgery mice were chronically implanted bi-laterally with Lambda-B Fibers (Optogenix) at 3.2 mm lateral from lambda, 300 μm rostral from the transverse sinus and inserted to a depth of ~2.5mm from the dorsal surface

of the brain. Fiber dimensions were as follows: NA = 0.39, core/cladding diameter = 200 μm/225 μm; Light Emitting Length = 2 mm; Implant Length = 1 mm. Following the surgery, a thin layer of metabond was applied to cover the brain, all exposed skull, the Lambda-B ferrule and support a titanium headplate (7 mm x 23 mm). Note, both fiber implant and viral injection pipette were inserted perpendicular to the lambda-bregma plane.

Behavior

All mouse behavior reported in this study were conducted using a custom MATLAB-based virtual reality environment (ViRMEn) previously described in Heys and Dombeck (2018). Briefly, mice were head-fixed over a cylindrical treadmill (19.7 cm diameter) and were free to run on the treadmill. Mouse movement on the treadmill was then translated into movement through a virtual linear 2-m track, displayed on 5 monitors contiguously positioned in a semi-circle around the mouse. Mouse locomotion speed on the treadmill was measured using a rotary encoder (E2-5000, US Digital). Movement gain was set such that the full length of the virtual track was 2 m of linear distance and the view angle in the virtual environment was fixed such that the mouse's view was always straight down the center of the track. The rotational velocity of the treadmill (directly related to the mouse's running speed on the treadmill) was linearly related to movement speed along the virtual track.

Pre-training Phase - linear track (no Door Stop) followed by a 2 s visible Door Stop task:

Approximately 1 week after viral injection surgery, mice first began training in a virtual linear track environment (no Door Stop). In the linear track task, mice began at the start of the 2-m track and ran down the track to obtain a small water reward (4 μL) at the end of the track. After the reward and a 2 s delay period, the mouse was ''teleported'' back to the start of the track to begin another traversal. Upon reaching criteria on the linear track task (> 1 reward/min), mice began training on a visible Door Stop task. At this stage in the training the experimenter was blinded to mouse type (JAWs or Control-EGFP). In the visible Door Stop, mice ran the linear track to a visible door located halfway down the 2-m track. At the door, the mice were required to stop for 2 s (locomotion double velocity threshold: V_1 = 1.5 cm/sec and V_2 = 5.5 cm/sec) within 10 cm of the door location. The double velocity threshold was set such that mouse velocity must first decrease below V_1 and subsequently remain below V_2 in order for the door to open. An instrumental cue in the form of an auditory click was presented to inform the mouse that the Door Stop timing period had begun. Only once the mice had stopped for a given interval did the door open, at which point they could run forward through the open door and travel another 1 m to the track end zone in order to gain a small water reward (4 μL). Because the treadmill was not fixed in place during the timing interval, the mice could begin running on the treadmill before the interval was complete. In such cases, the door did not open and the mice could not progress forward along the virtual track; once the mice stopped again, the interval started over with another auditory click sound.

Experimental Phase – 4 s Invisible Door Stop Task

Once mice reached criteria of > 1 reward/min on the 2 s visible Door Stop task, the mice were switched to the experimental phase (invisible Door Stop task). This task was identical to the visible door version of the task, except the door was made completely invisible and mice were required to wait for 4 s in order to open the door. Mice were therefore not able to visualize when the door was present or not, but when the door was present, it would block the forward progress of the mice down the track. Further, since the mice could not see the invisible door opening at the end of the 4 s interval, this Door Stop task therefore requires an internal temporal representation for efficient completion. Each behavioral session was 50 minutes in total duration, which was divided into a warm-up period that lasted for 10 minutes using a visible door with a 4 s wait (with no light delivery), followed by 40 minute period using an invisible door with a 4 s wait (with light delivery).

Optical inhibition of MEC neurons

During the experimental phase of the Door Stop task, continuous laser light (635nm diode laser, Thorlabs) was coupled to the Lambda-B fibers and delivered bi-laterally to MEC (Power = 8-9mW measured before coupling into the Lambda-B fiber coupler). During the temporal learning experiment, light delivery occurred during all wait periods when mice were stopped and positioned at the invisible door (Figure 2). During the spatial-learning experiment, light delivery occurred when mice traversed the second half of the linear track (after waiting at the door). On each lap in the spatial-learning experiment, the laser duration was chosen randomly from an exponential distribution with a mean of 3.33 s. This value was chosen to best match the duration of light delivery from the temporal learning experiments shown in Figure 2, and was obtained by measuring the mean wait time at the invisible door across all six behavioral sessions. In order to avoid disrupting reward mediated learning in this instrumental task, the light delivery ceased when mice approached within 10 cm from the reward zone, regardless of whether the chosen light delivery duration on that lap had been reached or not.

In order to confirm the efficacy of JAWs mediated inhibition, multi-unit recordings were conducted using bi-polar tungsten electrodes (1-2Mohm, WPI) and an extracellular amplifier (Model 1800, A-M Systems, x1000 gain, lowpass filter: 20KHz, highpass filter: 100Hz). Mice were injected with AAV8.hSyn.Jaws-KGC.GFP-ER2.WPRE.hGH (6 recording sessions across 4 mice) and subsequently implanted with a Lambda-B light fiber using the same protocol described above. 6-8 weeks after the injection, a surgery was performed to make a craniotomy located medial to the optical fiber. Following the surgery, mice were allowed to recover from anesthesia and were then head-fixed over a cylindrical treadmill for combined electrophysiological recordings and optogenetic

manipulations. Using stereotaxic alignment, the electrodes were then targeted to MEC. The location of the electrode was confirmed by advancing the electrode toward MEC and monitoring for laser induced changes in the multi-unit activity. Once the location of the electrode was positioned in MEC, recordings were initiated. During recordings, continuous light at 7-9 mW (measured as described above) was delivered to the Lambda-B fiber for 1-3 s durations followed by 5-10 s inter-trial interval, and repeated over 100 trials.

Histology

Following behavioral experiments, Lambda-B fibers were surgically removed. The mouse was then euthanized and the brain was removed and fixed in 4% PFA in 0.1M PBS for ~24 hours. The brains were then transferred into a 30% sucrose solution in 0.1M PBS for approximately 2 days until they sank in the solution. The tissue was sectioned in 50 micron sagittal slices using a freezing microtome. Free floating slices were then incubated 0.1M PBS with 0.1% Triton-X for 10 minutes, washing 3 times with 0.1M PBS and incubated for 1 hour in a 25:1 solution of 0.1M PBS with 435/455 blue or 530/615 red fluorescent Nissl stain (Invitrogen). Brain sections were imaged and stitched using a VS120 Virtual Slide fluorescence microscope (Olympus). MEC was identified based on the location of lamina dissecans, the post-rhinal border and the circular shape of the dentate gyrus shown at the medial-lateral position of the sagittal sections.

QUANTIFICATION AND STATISTICAL ANALYSIS

Statistical Tests

Details of statistical tests, number of observations, and p values are indicated in the figures and figure captions and within the text. P values less than 0.05 were considered significant.

Data Analysis

All behavioral data (Figures 2, 3, and 4) was collected using P-clamp (Axon Instruments) and sampled at 1000 Hz. All combined electrophysiological and optogenetic data (Figure 1) was collected using P-clamp (Axon Instruments) and sampled at 30 kHz. These data are then analyzed using custom software written in MATLAB (2018a,b). For multi-unit electrophysiological recordings, spikes were defined as contiguous voltage deflections that were > 3 standard deviations from the mean. The bin numbers for each histogram have been chosen by visual inspection to maximize wait-time resolution while minimizing noise. The number of bins are the same between groups in each figure panel. For Bayesian Estimation (Figures 2E and 3D), the posterior distributions for each difference in the means was estimated using hierarchical Markov chain Monte Carlo (MCMC) methods (Kruschke, 2015). Using the posterior distribution, the highest density interval (HDI) was defined as the set of values over which 95% of credibility is spread. All data in the text and figures are labeled as either mean ± s.d. or mean ± s.e.m.